Electrochemically induced CO_2 capture enabled by aqueous quinone flow chemistry

Yan Jing,[1,2,3,7] Kiana Amini,[2,4,7] Dawei Xi,[2] Shijian Jin,[2,5] Abdulrahman Alfaraidi,[2] Emily F. Kerr,[1,6] Roy G. Gordon,[1,2] ✉ Michael J. Aziz[2] ✉

1. Department of Chemistry and Chemical Biology, Harvard University, Cambridge, Massachusetts 02138, United States
2. John A. Paulson School of Engineering and Applied Sciences, Harvard University, Cambridge, Massachusetts 02138, United States
3. Present address: Department of Materials Science and Engineering, National University of Singapore, 117575, Singapore
4. Present address: Department of Materials Engineering, University of British Columbia, Vancouver, BC Canada V6T 1Z4
5. Present address: X, the moonshot factory, 100 Mayfield Ave., Mountain View, California, United States
6. Present address: Chemistry Department, Xavier University, 3800 Victory Parkway, Cincinnati, OH 45207, United States
7. These authors contributed equally to this work.

✉ E-mail: gordon@chemistry.harvard.edu; maziz@harvard.edu.

Abstract

Climate change caused by the accumulation of anthropogenic CO_2 emissions motivates the development and deployment of cost-effective, scalable, and energetically efficient techniques to capture CO_2 from point or diffuse sources. Electrochemically-driven CO_2 capture processes utilizing redox-active organics in aqueous flow chemistry show promise for nonflammability, continuous-flow engineering, and the possibility of being driven at high current density by inexpensive, clean electricity. We show that the deprotonated hydroquinone–CO_2 adducts, whose insolubility limits the utility of the quinone–hydroquinone redox couple, become soluble when alkylammonium cations are introduced. Consequently, we introduce alkylammonium groups to anthraquinone via covalent bonds, making the resulting bis[3-(trimethylammonio)propyl]-anthraquinones (BTMAPAQs) soluble. We report the first aqueous quinone flow chemistry-enabled electrochemical CO_2 capture process, which occurs at ambient temperature and pressure, and show that it proceeds via both a pH-swing and a nucleophilicity-swing mechanism. 1,5-BTMAPAQ reaches the theoretical capture capacity of two CO_2 molecules per quinone from 1-bar CO_2–N_2 mixtures for which the CO_2 partial pressure is as low as 0.05 bar, or the applied current density is as high as 100 mA/cm^2, or the organic concentration is as high as 0.4 M. The energetic cost ranges from 48 to 140 kJ/molCO_2. In a crude simulated flue gas composed of 3% O_2, 10% CO_2, and 87% N_2, 1,5-BTMAPAQ electrolyte reversibly captured and released 50% of the theoretical capacity during an exposure of over 4 hr. It outperforms its isomeric counterparts 1,4-, and 1,8-BTMAPAQ in capture capacity and O_2 tolerance, demonstrating a substituent position effect on the reactivity of isomers with CO_2 and O_2. The results provide fundamental insight into electrochemical CO_2 capture with aqueous quinone flow chemistry and suggest that oxygen tolerance of reduced quinones may be significantly advanced through molecular engineering.

Introduction

Accumulating atmospheric CO_2 concentrations from anthropogenic emissions compose the major source of global climate change. While progress is being made in switching from fossil fuel combustion to virtually emissions-free electricity sources, hard-to-abate sectors such as aviation and shipping will remain large sources of emissions for decades even in the most optimistic scenarios. Consequently, CO_2 removal – whether by capture from combustion exhaust or directly from the air or the ocean – is the subject of greatly increased attention, as it has become urgent to develop techniques that can be scaled up in a timely manner and globally deployed in the real world at reasonably low material and energetic cost.[1] Even after the attainment of a net zero emissions economy, it is likely that CO_2 removal will be desired in order to cut atmospheric concentrations toward pre-industrial levels. In an increasingly-electrified society, electrochemically-driven CO_2 capture at ambient conditions becomes an increasingly attractive option.

Quinones are ubiquitous electron-transfer carriers found in a range of living organisms.[2,3] Featuring structural diversity, richness, and tunability as well as the earth-abundance of the compositional elements (C, H, O, N, S), quinones have been used as industrial dyes and for large-scale industrial production of hydrogen peroxide.[4,5] Aqueous quinone flow batteries are approaching commercialization as a new generation of large-scale energy storage

technique.[6] Apart from energy storage, quinone cores can also be utilized for electrochemically induced carbon capture via two different mechanisms, depending on the use of solvents (Figure 1a). First, CO_2 can be directly chemisorbed by reduced quinones (Q^{2-}), forming adducts [$Q(CO_2)_2^{2-}$] in aprotic solvents.[7,8] Second, quinones can undergo proton-coupled electron transfer (PCET) to be reduced to the hydroquinone form (H_2Q) in protic solvents,[9] accompanied by the accumulation of hydroxide ions, indirectly leading to chemisorption of CO_2.[10,11] For both mechanisms, the captured CO_2 can be reversibly released upon electrochemical oxidation. For simplicity, we name the first (direct) capture mechanism the nucleophilicity-swing mechanism and the second (indirect) capture mechanism the pH-swing mechanism. In both cases, a CO_2 capture–release cycle involves quinone reduction (an electron transfer process, abbreviated as *E:* $Q + 2e^- \rightarrow Q^{2-}$; $Q + 2e^- + H_2O \rightarrow HQ^- + OH^-$; $Q + 2e^- + 2H_2O \rightarrow H_2Q + 2OH^-$), CO_2 absorption (a chemical reaction, abbreviated as *C:* $Q^{2-} + CO_2 \rightarrow Q(CO_2)_2^{2-}$; $HQ^- + CO_2 \rightarrow HQ(CO_2)^-$; $OH^- + CO_2 \rightarrow HCO_3^-$), and concerted electrochemical oxidation and CO_2 release (*E*: $Q(CO_2)_2^{2-} \rightarrow Q + 2CO_2 + 2e^-$; $HQ(CO_2)^- + HCO_3^- \rightarrow Q + H_2O + 2CO_2 + 2e^-$; $H_2Q + 2HCO_3^- \rightarrow Q + 2CO_2 + 2H_2O + 2e^-$). Therefore, both mechanisms undergo *ECE* processes in principle.

Quinones explored for CO_2 capture have been, almost without exception, immobilized on electrodes[12-15] or dissolved in organic electrolytes.[12,16,17] Solution-based capture inherits many of the advantages of flow batteries, including simple maintenance/top-off of active species, decoupled electrolyte activation and CO_2 capture, and continuous-flow engineering.[17,18] In particular, aqueous electrolytes possess the advantage[10,11,19-21] that water is non-flammable with virtually no cost; furthermore, high ionic conductivity of aqueous electrolytes allows high current density, enabling high areal throughput at ambient temperature and pressure. Combined, these advantages illustrate the opportunity for a capture system based on electrochemically-driven aqueous-soluble quinone flow chemistry. The sole aqueous-soluble quinone studied to date for CO_2 capture, disodium 4,5-dihydroxy-1,3-benzenedisulfonate (tiron), was studied only in static H-cells.[22,23] One CO_2 per quinone was released via pH-swing caused by the electrochemical oxidization of tiron. Unfortunately, more than 60% of the initial capacity was lost after the first cycle due to the instability of the oxidized tiron molecule, which undergoes Michael addition and subsequent polymerization. To our knowledge, aqueous quinone flow chemistry-enabled electrochemical CO_2 capture and release has not previously been demonstrated.

Theoretically, to utilize a quinone for PCET-mediated electrochemical CO_2 capture cycle in aqueous electrolyte, the initial pH of the quinone electrolytes should be somewhat below pK_{a1} of H_2CO_3 (~6), so that bicarbonate and carbonate concentrations are negligible compared to that of CO_2(aq). Upon electrochemical reduction, the quinone undergoes a PCET process, increasing the electrolyte pH until it reaches pK_{a2} of the corresponding H_2Q; upon further reduction of the electrolyte, the quinone undergoes zero-proton, two-electron transfer, generating Q^{2-} dianions without further altering the electrolyte pH.[9,24] Because H_2Qs are weak acids and their pK_a values are usually less than 13,[9,24,25] concentrated quinone electrolytes, when reduced, are expected to be predominantly in dianionic form rather than H_2Q form, favoring nucleophilicity-swing carbon capture. The two OH^- ions generated from the formation of hydroquinones would capture 1 or 2 CO_2 molecules via carbonate ($2OH^- + CO_2 \rightarrow H_2O + CO_3^{2-}$) or bicarbonate ($OH^- + CO_2 \rightarrow HCO_3^-$) formation. The two oxygen sites on the dianionic form of the reduced quinone can each bind one CO_2 molecule, yielding QCO_2^{2-} or $Q(CO_2)_2^{2-}$. Therefore, the CO_2 capture capacity of aqueous quinones is expected to range up to 2 CO_2 per quinone.

In general, aqueous quinones should meet several major criteria if used for electrochemical CO_2 capture. First, quinones should have high aqueous solubility in all states within their operational pH range. Second, the CO_2-reactive reduced species, including H_2Q, HQ^-, Q^{2-}, and $HQ(CO_2)^-$, $Q(CO_2)_2^{2-}$, should resist reaction with O_2 long enough for most of the CO_2 capture capacity to be realized. Additionally, for the adduct formation mechanism, rate constants should be reasonably high and the binding constants should be high enough for most of the maximum capture capacity of 2 CO_2 per quinone to be attained, but not so high as to lead to unnecessarily large adduct oxidation potentials.

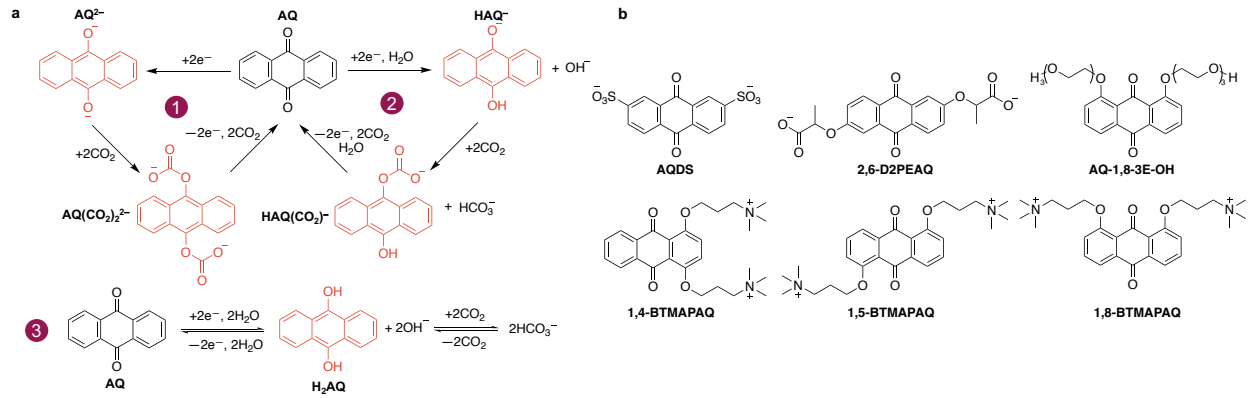

Figure 1 | (a) Aqueous anthraquinone electrochemical CO_2 capture mechanisms. (b) Six anthraquinone candidates that are soluble at neutral pH.

Aqueous soluble quinones

Informed by a decade of endeavors in developing aqueous anthraquinone flow batteries,[26-32] we selected three anthraquinone derivatives that are aqueous-soluble at neutral pH: 2,7-disulfonated anthraquinone (AQDS), 1,8-bis(2-(2-(2-hydroxyethoxy)ethoxy)ethoxy)anthracene-9,10-dione (AQ-1,8-3E-OH),[24] and 2,2′-((9,10-dioxo-9,10-dihydroanthracene-2,6-diyl)bis(oxy))-dipropionic acid (2,6-D2PEAQ)[33] (Figure 1b). Although those quinones show decent aqueous solubility in both oxidized and reduced states, bright yellow precipitates formed when CO_2 was introduced to the reduced electrolytes. The yellow precipitates did not form, and clear solutions were afforded when tetra-alkyl ammonium chlorides were used as the supporting salts (Figure 2, Table S1). Specifically, substituting 1 M NaCl with 1 M tetramethylammonium chloride (TMACl) as the supporting salt in 0.1 M AQDS electrolyte (Figure S1), replacing 1 M KCl with 1 M tetrabutylammonium chloride (TBACl) as the supporting salt in 0.1 M 2,6-D2PEAQ (Figure 2) or in 0.1 M AQ-1,8-3E-OH electrolytes produce transparent bright yellow solutions. One plausible explanation is that the bulky, amphiphilic tetra-alkyl ammonium cations and $Q(CO_2)_2^{2-}$ can form loose ion pairs rather than the tight ion pairs between alkali metal cations and $Q(CO_2)_2^{2-}$, thus drastically altering the solubility behavior.[34] However, the bulkiness of tetra-alkyl ammonium cations cause extremely high cell resistance (Figure S2a) in the flow cell systems because, in such cells, cation-exchange membranes must be used, resulting in prohibitively high energetic cost.

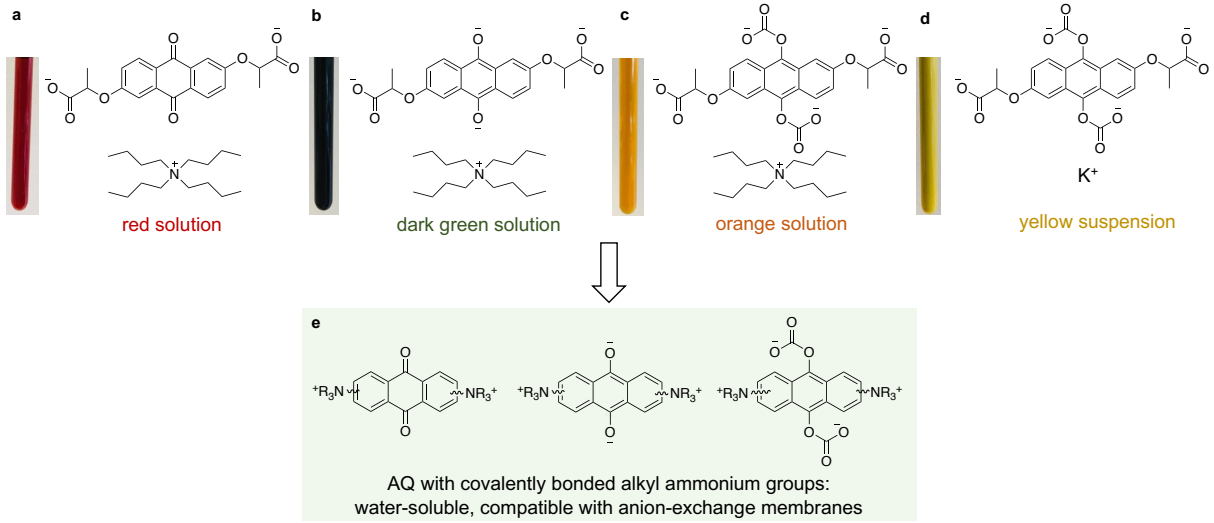

Figure 2 | Affect of supporting salt cations on solubility of $Q(CO_2)_2^{2-}$. (a) 0.1 M 2,6-D2PEAQ in 1 M TBACl; (b) 0.1 M reduced 2,6-D2PEAQ in 1 M TBACl; (c) 0.1 M reduced 2,6-D2PEAQ with saturated CO_2 in 1 M TBACl. (d) 0.1 M reduced 2,6-D2PEAQ with saturated CO_2 in 1 M KCl. (e) AQ possessing alkyl ammonium ending groups connected via covalent bonds, enhancing aqueous solubility and affording compatibility with anion-exchange membranes.

Inspired by the observation of dramatic change in aqueous solubility of reduced AQs in the presence of CO_2 caused by tetra-alkyl ammonium salts (Figure 2, Table S1), we hypothesized that anthraquinone derivatives tethered with bulky alkyl ammonium cations via covalent bonds might not only have high aqueous solubility in all states, but also be compatible with anion exchange membranes: the oxidized forms are positively charged and the reduced forms are charge-neutral but large in size, with correspondingly low expected cross-over rates. We designed and synthesized 1,4-, 1,5-, 1,8-,[35] and 2,6-bis[3-(trimethylammonio)propyl]-anthraquinone (BTMAPAQs) in which the numbers represent the positions of water-solubilizing chains (TMAP) bonded to anthraquinone (AQ) core. Of the four isomers, 2,6-BTMAPAQ exhibits very limited solubility (< 0.1 M) even in its oxidized state (Table S1); 1,8-BTMAPAQ$(CO_2)_2^{2-}$ becomes soluble when TBA^+ is used as the supporting salt cation (Figure S3); 1,4-, and 1,5-BTMAPAQs are soluble in all states even if KCl is used as the supporting salt. Therefore, 1,4-, 1,5-, and 1,8-BTMAPAQs (Figure 1b) were investigated for electrochemical CO_2 capture.

CO_2 capture mechanism verification

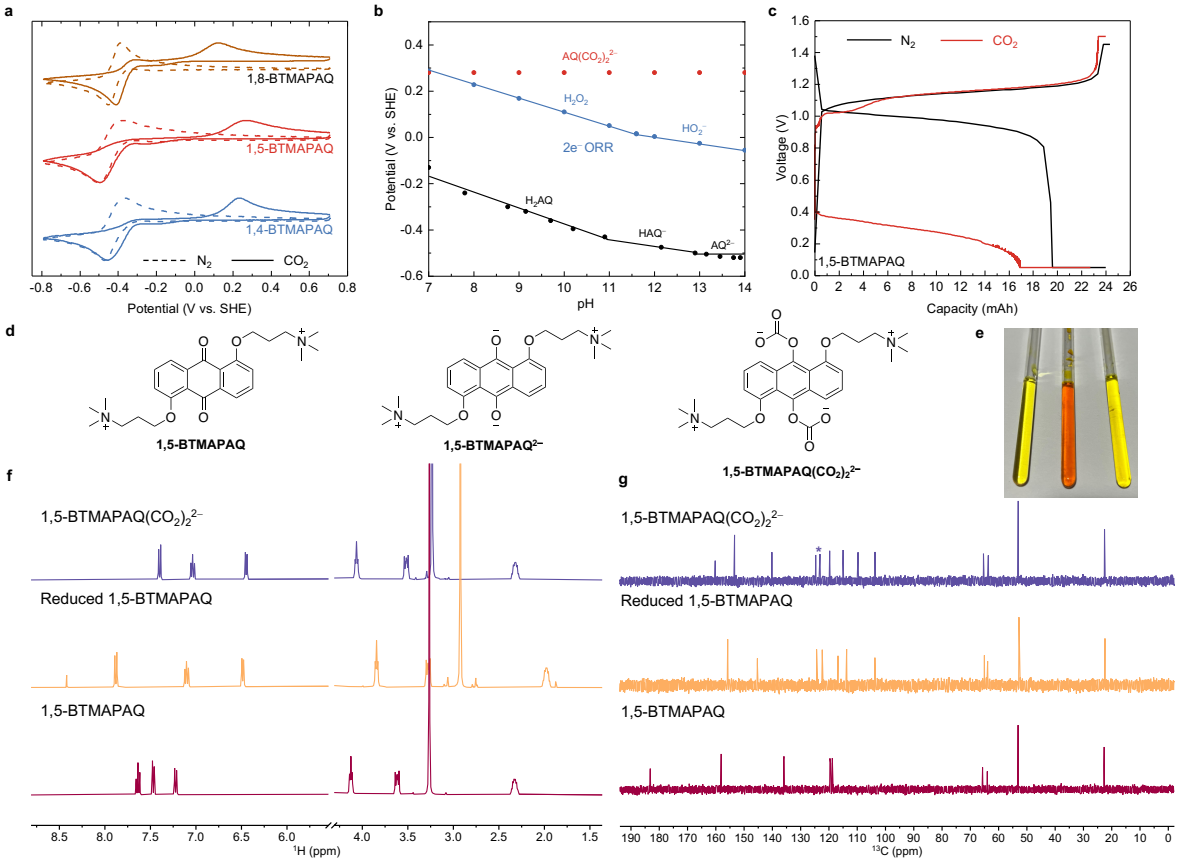

Figure 3 | Electrochemical and physiochemical characterization of BTMAPAQ in N_2 and CO_2. (a) Cyclic voltammogram (CV) of 10 mL, 5 mM 1,4-, (1,5-)BTMAPAQs in 1 M KCl, 5 mM 1,8-BTMAPAQ in 1 M KCl under streams of pure N_2 (dashed) or CO_2 (solid) at a scan rate of 100 mV s^{-1}. (b) Pourbaix diagram of 1,5-BTMAPAQ (AQ + $2e^-$ + $2H_2O$ → H_2AQ + $2OH^-$; AQ + $2e^-$ + H_2O → HAQ^- + OH^-; AQ + $2e^-$ → AQ^{2-}) and 2-electron oxygen reduction reaction ($½O_2 + 2e^- + H_2O$ → H_2O_2; $½O_2 + 2e^- + H_2O$ → $HO_2^- + H^+$). (c) Voltage profiles of 1,5-BTMAPAQ | FcNCl in 100% N_2 (black) and 10% CO_2 + 90% N_2 for (red). (d) Structure of 1,5-BTMAPAQ, 1,5-BTMAPAQ^{2-}, and 1,5-BTMAPAQ$(CO_2)_2^{2-}$. (e) NMR specimens, from left to right in the same order as the molecular structures in (d), and their ^1H NMR (f) and ^{13}C NMR (g) spectra. Note that ^1H NMR peak broadening was initially observed from the electrochemically reduced aqueous quinone due to the occurrence of residual radicals, but addition of a tiny amount of HCl afforded well-defined peak splitting in the aromatic region (Figure 3f, orange). The chemical shift at 124.6 ppm in 1,5-BTMAPAQ$(CO_2)_2^{2-}$ (Figure 3g, purple, identified with asterisk) is from the dissolved CO_2.[36]

Cyclic voltammetry (CV) was employed to investigate BTMAPAQs in buffered and unbuffered solutions. As shown in Figure 3a, at pH 7 in N_2, 1,5-BTMAPAQ exhibits a redox potential of −0.465 V vs. SHE with a peak separation of 90 mV. When the solution was constantly purged with CO_2, the major cathodic peak appears at −0.51 V along with a minor cathodic peak at −0.28 V (Figure 3a), which might be caused by a CO_2 buffering effect, enabling 1,5-BTMAPAQ to partially undergo a PCET process.[9] The anodic peak of 1,5-BTMAPAQ largely shifts to +0.28 V, suggesting that extra energy is required to trigger the electrochemical oxidation: 1,5-BTMAPAQ$(CO_2)_2^{2-}$ → 1,5-BTMAPAQ + $2CO_2$ + $2e^-$. Similar electrochemical behaviors were also shown by 1,4- and 1,8-BTMAPAQs.

To extract the relationship between redox potentials of 1,5-BTMAPAQ and electrolyte pH, we ran CVs in a series of buffered electrolytes to plot its Pourbaix diagram (Figure 3b). The pKa_1 and pKa_2 of 1,5-BTMAPH_2AQ are estimated at 10.9 and 12.8, consistent with other aqueous soluble anthrahydroquinones (H_2AQ).[24,25,33] Because of the dominance of the nucleophilicity-swing mechanism in concentrated solutions, hereafter the oxidized, reduced, and CO_2 bonded states of quinones are abbreviated as Q, Q^{2-}, and $Q(CO_2)_2^{2-}$.

We assembled BTMAPAQs | (ferrocenylmethyl)trimethylammonium Chloride (FcNCl)[37] flow cells separated by anion-exchange membranes. Thanks to the compatibility between membrane and electrolytes, the alternating current area-specific resistance of the cells, measured via high-frequency electrochemical impedance spectroscopy, is as low as ~1.5 Ω cm^2 (Figure S4). While operating in 0.1 bar CO_2 and 0.9 bar N_2, we noticed a distinct discharge voltage decrease (Figure 3c, Figure S5), consistent with the anodic peak shifts in CVs (Figure 3a), confirming that $Q(CO_2)_2^{2-}$ is the major product when the reduced form is exposed to CO_2. Interestingly, the color of BTMAPAQ solution changed dramatically in different states. For instance, 1,5-BTMAPAQ solution turned from bright yellow to light orange to pale yellow, corresponding to 1,5-BTMAPAQ, 1,5-BTMAPAQ^{2-}, and 1,5-BTMAPAQ$(CO_2)_2^{2-}$ (Figure 3e); the structure change was reflected by the distinct chemical shifts in both ^1H and ^{13}C NMR spectra (Figure 3f, 3g). Dramatic color changes as well as distinct chemical shifts were also exhibited by AQDS and 1,8-BTMAPAQ in their corresponding three states (Figure S1, S3).

Electrochemical CO_2 capture and release

To examine the CO_2 capture capability of BTMAPAQs, we first conducted chemically induced CO_2 capture from pure, flowing CO_2, release into N_2, and sequestration as $BaCO_3$(s), from which we validated the CO_2 capture capacity of two CO_2 per quinone (Figure S6). Subsequently, we investigated the electrochemically induced CO_2 capture performance of 1,5-BTMAPAQ at 0.5 bar CO_2 and 0.5 bar N_2. (Figure 4a). The electrochemical reduction and oxidation were accompanied by CO_2 capture and release, which were reflected by the periodic oscillation of downstream CO_2 partial pressure and downstream gas flow rate, as well as the pH swing of 1,5-BTMAPAQ electrolyte. A 45-min. interval between reduction and oxidation was chosen as the minimum rest time to complete the gas-liquid reaction, which is the rate-limiting step (Figure S7). Integrating the downstream gas flow rate change during the CO_2 release indicates that the measured volume of released CO_2 is almost the same as the theoretical value (Figure S8), suggesting that each 1,5-BTMAPAQ can capture and release two CO_2 molecules. Through analyzing the round-trip voltage efficiency and coulombic efficiency over five cycles of the electrochemical reduction and oxidation, we found the energetic cost ranges from 65 to 80 kJ/molCO_2 at 20 mA/cm^2 at a fixed inlet CO_2 partial pressure of 0.5 bar. The close correspondence between the coulombic efficiency and the CO_2 release/capture efficiency in Figure S8e, defined as the ratio of the amount of CO_2 released to the amount captured in the immediately preceding half-cycle, indicates that CO_2 capture/release is triggered by the electrochemical reactions and mirrored by coulombic efficiencies.

In real applications, the partial pressure of CO_2 in feed gas varies over a broad range; hence we performed a series of tests in feed gas with varied partial pressure of CO_2 at 0.05, 0.1, 0.2, and 0.5 bars. To increase the CO_2 capture capacity, we adjusted the corresponding rest time intervals as 210, 105, 52, and 45 min., respectively (Figure 4a, Figure S9). During the electrochemical reduction of 1,5-BTMAPAQ, the pH range went from wide to narrow while the CO_2 partial pressure was adjusted from 0.05 to 0.5 bar. For instance, the pH swung from near neutral to ~12 at 0.05 bar CO_2, but to only ~9 at 0.5 bar CO_2. According to Henry's law, a higher partial pressure of CO_2 can lead to a higher CO_2 solubility in solution, thus enabling the prompt buffering of pH increase induced by electrochemical reduction. Despite of the variation in CO_2 partial pressure, two CO_2 molecules were captured by one 1,5-BTMAPAQ with energetic cost of 48 to 50 kJ/molCO_2 at 20 mA/cm^2.

One advantage of aqueous flow chemistry is the capability to operate electrochemical reactions at high current densities. Although extremely diluted CO_2 essentially limits the CO_2 capture heterogeneous chemical reaction rate regardless of technology, CO_2 release in our system is coupled with electrochemical oxidation; thus the CO_2 release rate can be readily accelerated by applying high current densities. We electrochemically reduced and oxidized 1,5-BTMAPAQ at 20, 40, 60, 80, and 100 mA/cm^2 in the presence of 0.1 bar CO_2 (Figure 4b, Figure S10). The depression of downstream CO_2 partial pressure and gas flow rate caused by CO_2 capture was almost the same at different current

densities, indicating that CO_2 capture reaction rate is limited by mass transport of 0.1 bar CO_2 rather than by the electrochemical reduction rate, i.e. the applied current density. However, the peaks of downstream CO_2 partial pressure and gas flow rate caused by CO_2 release became sharper and narrower with the increase of current density, suggesting that the CO_2 release rate can be accelerated with increased current density, thus shortening the CO_2 release time. It is worth noting that the calculated volumes of the released CO_2 reach the theoretical values at different current densities (Figure S10). The mid-point voltage difference between charge and discharge curves increases with current density, which is caused by internal cell resistance, resulting in a broad energetic cost range of 65 to 140 kJ/molCO_2.

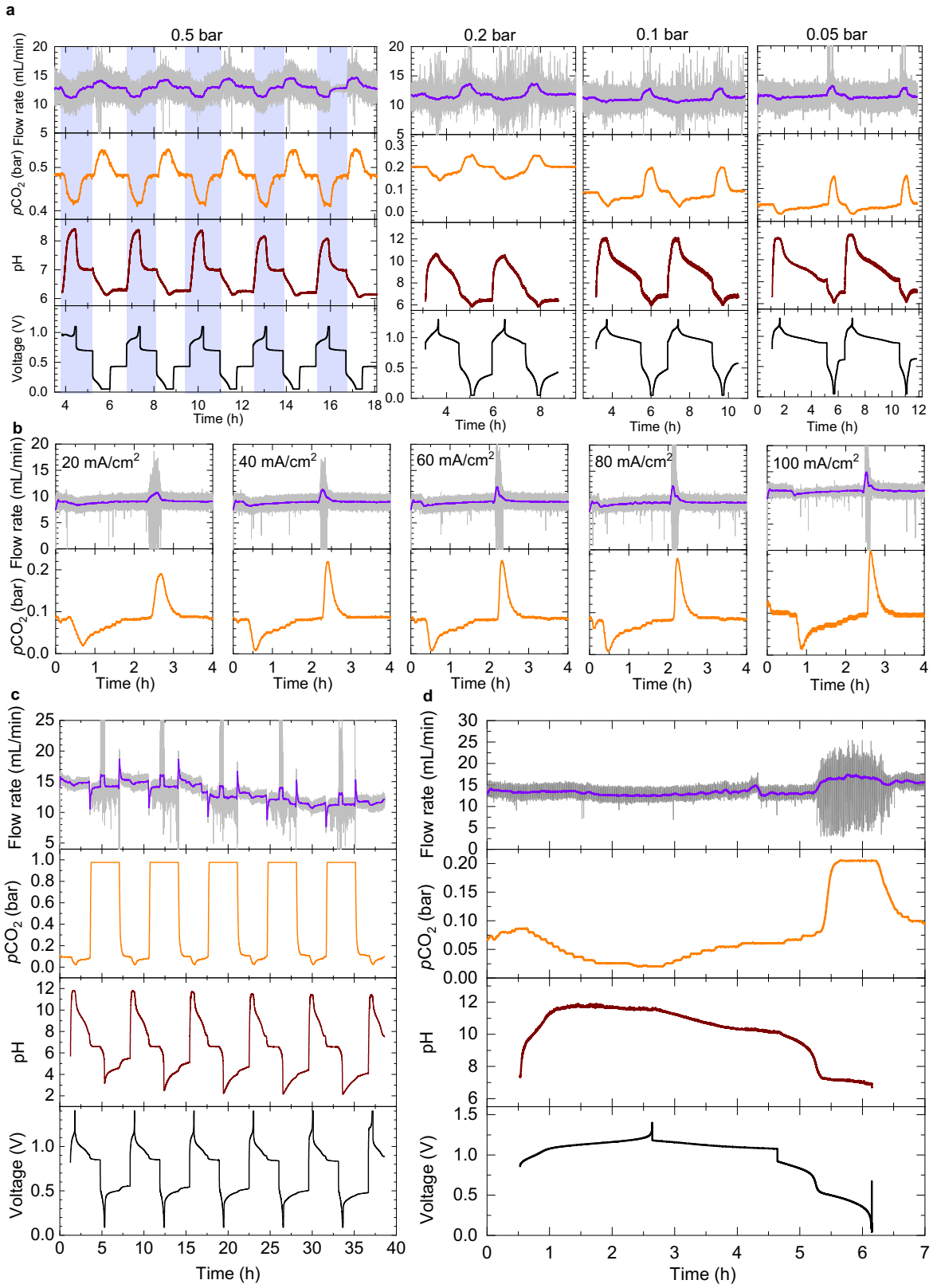

Figure 4 | 1,5-BTMAPAQ electrochemical CO_2 capture capability in CO_2–N_2 mixtures. (a) CO_2 capture and release cycling at 20 mA/cm^2. The partial pressure of CO_2 is set to ≈ 0.05, 0.1, 0.2, and 0.5 bar for the experiments,

separately. Flow cells comprising 10–12 mL of 0.115 M 1,5-BTMAPAQ in 1 M KCl and 40 mL of 0.2 M FcNCl in 1 M KCl were used for the experiments at 0.05, 0.1 and 0.2 bar. A flow cell comprising 10 mL of 0.115 M 1,5-BTMAPAQ in 1 M KCl and 40 mL of 0.2 M BTMAPFc (bis((3-trimethylammonio)propyl)ferrocene dichloride)[38] in 1 M KCl was used for the experiment at 0.5 bar. (b) Plot presents the downstream CO_2 partial pressure and the downstream total gas flow rates when the electrochemical redox reactions were triggered at 20, 40, 60, 80, and 100 mA/cm^2. A flow cell comprises 10 mL of 0.057 M 1,5-BTMAPAQ in 1 M KCl and 40 mL of 0.1 M FcNCl in 1 M KCl. (c) CO_2 capture and release cycling where the capture occurred in an inlet CO_2 partial pressure of 0.1 bar and the release occurred in an inlet CO_2 partial pressure of 1 bar. A flow cell comprises 12 mL of 0.115 M 1,5-BTMAPAQ in 1 M KCl and 40 mL of 0.2 M FcNCl in 1 M KCl at 20 mA/cm^2. (d) CO_2 capture and release in inlet CO_2 partial pressure of 0.1 bar in a flow cell comprising 10 mL of 0.4 M 1,5-BTMAPAQ DI water and 30 mL of 0.9 M FcNCl in DI water at 20 mA/cm^2. Plots present current density, voltage, pH, downstream CO_2 partial pressure, and the downstream total gas flow rate of 1,5-BTMAPAQ electrolyte. The initial gas flow rate is set to 11.76 mL/min.

It is important to evaluate the CO_2 capture capacity and energetic cost when a system is used to capture CO_2 from a diluted source and release pure CO_2. Hence, we performed our experiment using 1,5-BTMAPAQ with 0.1 bar inlet CO_2 and 1.0 bar pure CO_2 exit stream (Figure 4c). The volume of released CO_2 approaches the theoretical value over five cycles (Figure S11). The energetic cost and coulombic efficiency are either comparable to or slightly higher than those measured under previous conditions (Figure S9, S10).

A concentrated quinone flow system comprising 0.4 M 1,5-BTMAPAQ was set up to demonstrate high volumetric CO_2 capture capacity (Figure 4d). Because of the low p*K*a values (<13) of 1,5-BTMAPH_2AQ (Figure 3b), the pH swing for 0.4 M 1,5-BTMAPAQ is the same as that for 0.1 M 1,5-BTMAPAQ, further supporting our interpretation of the results as the formation of $Q(CO_2)_2^{2-}$. Although the increased concentration of 1,5-BTMAPAQ took a longer time to complete the capture, it still reaches the theoretical capacity at the energetic cost of 90 kJ/molCO_2.

O_2 sensitivity evaluation

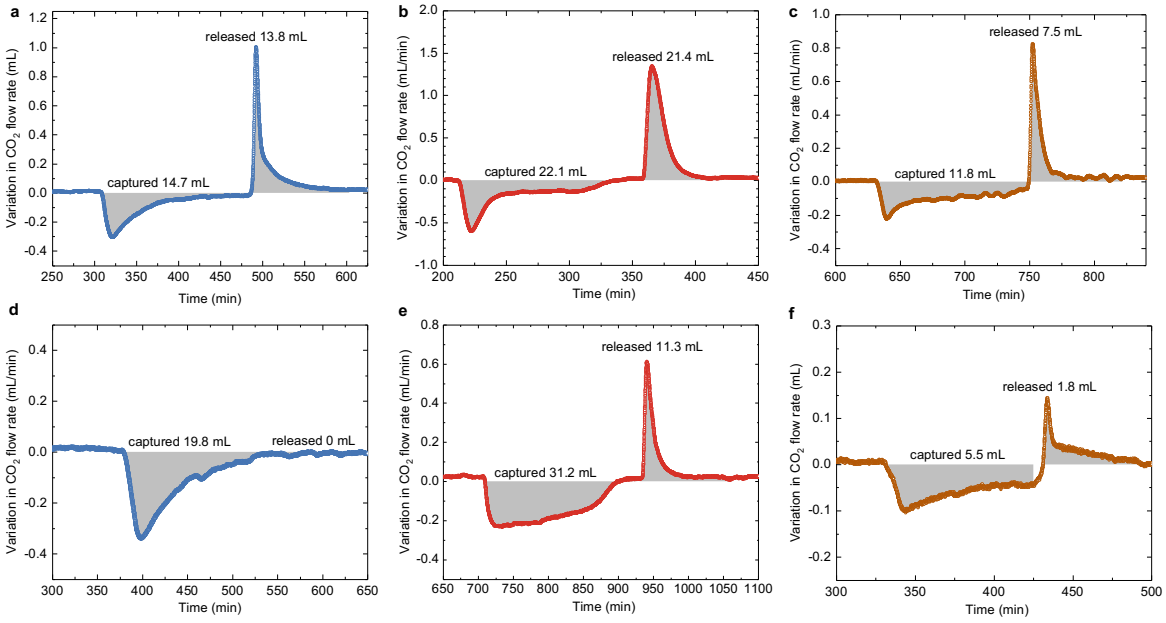

Figure 5 | CO_2 capture and release of 1,4-, 1,5-, 1,8-BTMAPAQs with and without O_2. Calculated volumes of captured and released CO_2 by (a) 1,4-, (b) 1,5-, (c) 1,8-BTMAPAQs in a feed gas stream of 90% N_2 and 10% CO_2 at 1.0 bar. Calculated volumes of captured and released CO_2 by (d) 1,4-, (e) 1,5-, (f) 1,8-BTMAPAQs in a feed gas stream of 87% N_2, 10% CO_2, and 3% O_2 (simulated flue gas) at 1.0 bar. 5 mL 0.1 M 1,4-, 1,5-BTMAPAQs, 1 M KCl solutions were paired with 40 mL 0.1 M FcNCl, 1 M KCl solution. 5 mL 0.1 M 1,8-BTMAPAQ 1 M TBACl solution was paired with 40 mL 0.1 M FcNCl, 1 M TBACl solution. The BTMAPAQs were electrochemically reduced and oxidized at 40 mA/cm^2 and followed by potential holds to complete the reactions. The theoretical CO_2 capture & release capacity for the BTMAPAQ electrolytes is 22.4 mL. Electrochemical reduction/oxidation were followed by rest time that was adjusted to approach the maximum CO_2 capture/release capacity while minimizing the O_2 induced side reactions. The durations of CO_2 capture/release for 1,4-BTMPAQ are 175/125 min. without O_2 and 170/100 min.

in the simulated gas, respectively. The durations of CO_2 capture/release for 1,5-BTMPAQ are 145/80 min. without O_2 and 226/160 min. in the simulated gas, respectively. The durations of CO_2 capture/release for 1,8-BTMPAQ are 120/90 min. without O_2 and 100/70 min. in the simulated gas, respectively. The addition of 1 M TBACl to 0.1 M 1,8-BTMAPAQ increased the viscosity of solution, slowing the dissolution of CO_2 and O_2 from gas phase to liquid phase.

In real applications, CO_2 always coexists with O_2 at varying partial pressures depending on CO_2 sources. It has been reported that reduced quinones are susceptible to O_2,[17,39,40] which can reversibly chemically oxidize the reduced quinones to their oxidized states. These reduced quinones are the species of interest for binding CO_2. Hence, we investigated the oxygen sensitivity of the reduced quinones including H_2Q, HQ^-, Q^{2-}, $HQ(CO_2)^-$, and $Q(CO_2)_2^{2-}$, as capture will become practical only if the reduced quinones become oxidized by O_2 sufficiently slowly in an atmosphere with a relatively high O_2 partial pressure.

The reduced quinones are oxygen-sensitive because their oxidation potentials are much lower than the O_2 reduction potential. Whereas the oxidation potentials of $Q(CO_2)_2^{2-}$ can positively shift by at least 500 mV compared to those of the reduced quinones (Figure 3a), approaching the reduction potential of O_2 (Figure 3b), which may make $Q(CO_2)_2^{2-}$ more O_2-tolerant. Through tracking ^{1}H NMR of the reduced quinones with and without captured CO_2 during air exposure (Figure S13–S18), we observed the reduced quinones gradually converted to the oxidized forms over days with different conversion rates. After operating BTMAPAQ flow cells in atmospheres with fixed CO_2 partial pressure but varied O_2 partial pressure (Table S2), we analyzed their coulombic efficiency to compare the oxygen sensitivity of BTMAPAQ isomers. We also performed chemically induced CO_2 capture, release, and sequestration with air exposure (Figure S19) and found that 1.7 equivalents of CO_2 were released when the solution with captured CO_2 was vigorously stirred in air for 15 min. The detailed information is reported in the Oxygen sensitivity section of Supplementary Information. Those measurements inspired us to further evaluate BTMAPAQs-based electrochemical CO_2 capture from simulated flue gases with an upgraded system setup (Figure S20–S22). By integrating the peak area of CO_2 flow rate deviation over CO_2 capture and release cycles (Figure 5), we evaluated the CO_2 capture and release volumes from 1,4-, 1,5-, and 1,8-BTMAPAQs in the absence and presence of O_2. When 1,4- and 1,5-BTMAPAQ were exposed to 1.0 bar feed gas composed of 10% CO_2 and 90% N_2, the CO_2 release/capture volume ratio is close to 1 (Figure 5a, 5b), suggesting the reversibility of CO_2 capture and release. When exposed to 1.0 bar simulated flue gas composed of 3% O_2, 10% CO_2, and 87% N_2, the volumes of released CO_2 greatly decrease, which we attribute to the oxygen-induced side reactions shown in Eqns. 10 and 11 in Table 1. Compared to the CO_2 capture volumes from 1,4- and 1,5-BTMAPAQs in the absence of O_2, their CO_2 capture volumes in the presence of O_2 become significantly larger, which we attribute to additional CO_2 irreversibly trapped by the hydroxide ions converted from oxygen (Eqns. 7, 8, 10, and 11 in Table 1). The CO_2 capture volumes from 1,8-BTMAPAQ are much smaller than those from 1,4- and 1,5-BTMAPAQ, which we tentatively attribute to the increased electrolyte viscosity caused by the addition of 1 M TBA^+, which slows down the dissolution of CO_2 to the electrolyte, lowering the capture capacity.

Among the three BTMAPAQ isomers, 1,5-BTMAPAQ shows the highest CO_2 capture capacity of 21.4 mL in the absence of O_2, which is close to the theoretical value of 22.4 mL assuming one 1,5-BTMAPAQ captures two CO_2 molecules. Under 3% O_2 exposure for 226 min. during CO_2 capture and 160 min. during the release, 1,5-BTMAPAQ still released 11.3 mL CO_2, which is ~50% of the theoretical capacity. It is worth noting that the CO_2 capture/release capacity can be further improved by optimizing the CO_2 capture time duration, as with decreased exposure time there should be fewer O_2-induced side reactions, and more captured CO_2 will be released. However, if the CO_2 capture duration is too short, both captured and released CO_2 volumes will become small, lowering the faradaic efficiency, defined in this context as the ratio of the amount of CO_2 reversibly captured and released to the theoretical capacity. Thus, a trade-off is apparent between the CO_2 release/capture volume ratio and faradic efficiency. Nevertheless, the O_2 resistance and CO_2 capture capability shown by 1,5-BTMAPAQ in Figure 4e demonstrates that reduced quinones are not necessarily too oxygen-sensitive to be useful for CO_2 capture. The BTMAPAQ-based electrochemical CO_2 capture–release behavior in a simulated flue gas atmosphere over multiple cycles (Figure S23–S26) illustrates that there is still room for improvement of long-term O_2-tolerance of reduced quinones through judicious molecular design. The distinct O_2 reactivity difference among the isomers implies that a substituent position effect plays a major role in governing their oxygen tolerance. This may be significantly improved via molecular engineering with the incorporation of steric and electronic effects, intra-, inter-molecular interactions, *etc*. induced by quinone cores or covalently bonded functional groups.

Table 1 | Electrochemical and chemical reactions during CO_2 capture & release when oxygen is involved. The hydroxide ions produced from Eqns. 7 and 8 can irreversibly capture CO_2 via Eqn 6.

Stage 1	Electrochemical reduction	Eqn. 1	$AQ + 2e^- \rightarrow AQ^{2-}$
		Eqn. 2	$AQ + 2e^- + 2H_2O \rightarrow H_2AQ + 2OH^-$
		Eqn. 3	$AQ + 2e^- + H_2O \rightarrow HAQ^- + OH^-$
Stage 2	Electrochemically induced CO_2 capture	Eqn. 4	$AQ^{2-} + CO_2 \rightarrow AQ(CO_2)_2^{2-}$
		Eqn. 5	$HAQ^- + CO_2 \rightarrow HAQ(CO_2)^-$
		Eqn. 6	$OH^- + CO_2 \rightarrow HCO_3^-$
	O_2-induced chemical reactions and irreversible CO_2 capture	Eqn. 7	$AQ^{2-} + H_2O + 1/2O_2 \rightarrow AQ + 2OH^-$
		Eqn. 8	$HAQ^- + 1/2O_2 \rightarrow AQ + OH^-$
		Eqn. 9	$H_2AQ + 1/2O_2 \rightarrow AQ + H_2O$
		Eqn. 10	$HAQ(CO_2)^- + 1/2O_2 \rightarrow AQ + OH^- + CO_2$
		Eqn. 11	$AQ(CO_2)_2^{2-} + H_2O + 1/2O_2 \rightarrow AQ + 2OH^- + 2CO_2$
Stage 3	Electrochemically induced CO_2 release	Eqn. 12	$AQ(CO_2)_2^{2-} - 2e^- \rightarrow AQ + 2CO_2$
		Eqn. 13	$H_2AQ - 2e^- + 2HCO_3^- \rightarrow AQ + 2H_2O + 2CO_2$
		Eqn. 14	$HAQ(CO_2)^- - 2e^- + HCO_3^- \rightarrow AQ + H_2O + 2CO_2$

Conclusions

Through molecular screening and modification, we developed three water-soluble and anion-exchange membrane compatible bis[3-(trimethylammonio)propyl]-anthraquinone (BTMAPAQ) isomers that can be used for electrochemical CO_2 capture. With a series of characterizations including cyclic voltammetry, Pourbaix diagram analysis, ^1H and ^{13}C NMR, electrochemical charge–discharge voltage–capacity profiles, and *in situ* monitoring of pH, p_{CO2}, and gas flow rate, we showed that aqueous quinone flow chemistry-enabled electrochemical CO_2 capture proceeds via pH-swing and nucleophilicity-swing mechanisms. The latter is more dominant because of low p*K*a values of hydroquinones. 1,5-BTMAPAQ electrolyte can capture and release the theoretical limit of two equivalents of CO_2 molecules per quinone from 1-bar CO_2-N_2 mixtures for which the CO_2 partial pressure is as low as 0.05 bar, or the applied current density is as high as 100 mA/cm^2, or the organic concentration is as high as 0.4 M, with an energetic cost ranging from 48 to 140 kJ/molCO_2. When exposed to a simulated flue gas comprising 3% O_2, 10% CO_2, and 87% N_2 at 1.0 bar total pressure for over 4 hr., 1,5-BTMAPAQ reversibly captured and released 50% of the theoretical capacity. The distinct position effect on O_2 reactivity exhibited by BTMAPAQ isomers illustrates the opportunity for molecular engineering for further improvement of molecular properties. This may stimulate the progress of oxygen-tolerant, low-cost, scalable aqueous quinone flow chemistry enabled electrochemical CO_2 capture.

Acknowledgments

Research at Harvard was supported by the Harvard Climate Change Solutions Fund. K.A. was supported in part by U.S.DOE award DE-AC05-76RL01830 through PNNL subcontract 654799 and in part through the Natural Sciences and Engineering Research Council of Canada (NSERC) Postdoctoral Fellowship (PDF) program [application number PDF-557232-2021]. We acknowledge Alex Forse from Univ. of Cambridge for useful discussions. We thank Prof. Theodore A. Betley, Dr. Thomas Cochard, Andrew Bergman, Toly Rinberg, Eric M. Fell, Thomas Y. George, Maia Alberts, Michael Emanuel, Dr. Jinxu Gao for useful discussions.

Author contributions

M.J.A. and R.G.G. supervised the project. Y.J., K.A., and M.J.A. conceived the idea. Y.J. and K.A. designed the experiment. K.A. performed the electrochemical CO_2 capture experiments in the absence of O_2 and analyzed the data. Y.J. designed and synthesized the molecules, performed the chemical characterizations, and ran electrochemical CO_2 capture experiments in the presence of O_2, and analyzed the data. D.X. and S.J. built the CO_2 capture setup and compiled the Arduino code for sensor control and data collection. A.A. collected the Pourbaix diagram data. E.F.K. synthesized the 2,6-D2PEAQ molecule. All authors contributed to the discussion. Y.J., K.A. and M.J.A. wrote the manuscript with input from all co-authors.

Experiments and methods

Synthesis of BTMAPAQs

To a 1 L of flame dried Schlenk flask, 40 mmol of dihydroxyanthraquinone, 88 mmol of anhydrous K_2CO_3, and 9.5 mmol of KI were suspended in 160 mL of anhydrous DMF. After being stirred under nitrogen for 20 min., 88 mmol of 3-bromopropyl trimethylammonium bromide was added to the dark suspension. The dark suspension was sealed to prevent ambient moisture, then was vigorously stirred at 100 ˚C for 16 hours to afford a brownish slurry.

After being cooling down, the slurry was added with 150 mL of ethyl acetate, stirred at room temperature for 30 min., then filtered to collect the brown cake. The washing procedure was repeated for few times until the filtrate became colorless. The cake was dissolved into methanol, and the solution was filtered to remove insoluble inorganic salts. The filtrate was condensed under vacuo to remove methanol and collect the dark red solid, which was then redissolved in deionized water.

The aqueous quinone solution was then transferred to an anion-exchange resin column prepared in advance to replace bromide with chloride ions. The dark red (bright yellow depending on the concentration) solution was condensed under vacuo to remove water and collect the red solid.

The red solid was re-dissolved in methanol to get the saturated solution, which was then drop-wise added to 200 mL of ethyl acetate and afford precipitates. The precipitates were collected by filtration to get final orange to yellow cakes. The yields range from 85% to 95%.

Characterization

^{1}H, ^{13}C NMR spectra were recorded on Varian INOVA 500 spectrometers at 500 MHz. Aliquots were prepared in deuterated water (D_2O), corresponding NMR spectra were recorded in D_2O with the residual H_2O (δ 4.79 ppm for ^{1}H NMR).
Electrochemical characterizations

Cyclic voltammetry measurements

Glassy carbon was used as the working electrode for all three-electrode CV tests with a 5 mm diameter glassy carbon working electrode, an Ag/AgCl reference electrode (BASi, pre-soaked in 3 M NaCl solution), and a graphite counter electrode. All cyclic voltammetry, linear sweep voltammetry, and chronoamperometry measurements were conducted on Gamry Instruments and CHI Instrument electrochemical analysers.

Flow cell assembly

Flow cell experiments were constructed with cell hardware from Fuel Cell Tech (Albuquerque, NM). The flow cell was assembled into a zero-gap flow cell configuration using pyrosealed POCO graphite flow plates with identical interdigitated flow fields. Each electrode was composed of 1 layer of AvCarb HCBA carbon cloth with a 5 cm^2 geometric surface area. Selemion DSV-N was used as the anion exchange membrane. The flow rate was set at 50–70 mL/min. Biologic SP-150e and Gamry Reference 3000 potentiostat was used as our electrochemical workstation. KNF diaphragm pumps were used to circulate electrolytes through the flow fields and electrodes in the cell stack. For some tests, a Cole-Parmer Digital gear pump was used.

Bis((3-trimethylammonio)propyl)ferrocene dichloride (BTMAPFc) and (ferrocenylmethyl)trimethylammonium Chloride (FcNCl) were purchased from TCI-America chemical company. Tetramethyl ammonium chloride, tetrabutylammonium chloride were purchased from Sigma Aldrich. All those chemicals were directly used without further purification.

Electrochemical CO_2 capture and release

Flow cells were charged at constant current, followed by voltage holds until current hits the background current values. Then the flow cells were set in rest mode for certain time to complete carbon capture. The cells were discharged at constant current, followed by a voltage hold. After the voltage hold, the battery was set in rest mode to complete CO_2 release.

A stream of feed gas composed of N_2, CO_2, and O_2 was introduced to the anthraquinone electrolytes and kept flowing constantly with pre-set partial pressure. The total pressure is 1 bar, and the total flow rate is 11.76 mL/min.
FS4001 MEMS Mass Flow Sensor, LuminOX O_2 sensor (CM-42990), SprintIR CO_2 sensor (GC-0018) were used in our tests.

References

[1]K.Z. House, A.C. Baclig, M. Ranjan, E.A. van Nierop, J. Wilcox, and H.J. Herzog, "Economic and energetic analysis of capturing CO_2 from ambient air", *Proc. Natl. Acad. Sci. U S A* **108**, 20428 (2011). https://doi.org/10.1073/pnas.1012253108

[2]P.J. O'Brien, "Molecular mechanisms of quinone cytotoxicity", *Chem.-Biol. Interactions* **80**, 41 (1991). https://doi.org/https://doi.org/10.1016/0009-2797(91)90029-7
[3]B. Nowicka and J. Kruk, "Occurrence, biosynthesis and function of isoprenoid quinones", *Biochim Biophys Acta* **1797**, 1587 (2010). https://doi.org/10.1016/j.bbabio.2010.06.007
[4]B. Dulo, K. Phan, J. Githaiga, K. Raes, and S. De Meester, "Natural quinone dyes: A review on structure, extraction techniques, analysis and application potential", *Waste and Biomass Valorization* **12**, 6339 (2021). https://doi.org/10.1007/s12649-021-01443-9
[5]J.M. Campos-Martin, G. Blanco-Brieva, and J.L. Fierro, "Hydrogen peroxide synthesis: An outlook beyond the anthraquinone process", *Angew. Chem. Int. Ed. Engl.* **45**, 6962 (2006). https://doi.org/10.1002/anie.200503779
[6]Y. Jing, R.G. Gordon, and M.J. Aziz, "Aqueous organic flow batteries.", *Weinheim: Wiley-VCH* **3**, (2023).
[7]M.B. Mizen and M.S. Wrighton, "Reductive addition of CO_2 to 9,10-phenanthrenequinone", *Journal of the Electrochemical Society* **136**, 7 (1989). https://doi.org/https://doi.org/10.1149/1.2096891
[8]P. Scovazzo, J. Poshusta, D. DuBois, C. Koval, and R. Noble, "Electrochemical separation and concentration of 1% CO_2 from nitrogen", *Journal of the Electrochemical Society* **150**, 8 (2003). https://doi.org/https://doi.org/10.1149/1.1566962
[9]M. Quan, D. Sanchez, M.F. Wasylkiw, and D.K. Smith, "Voltammetry of quinones in unbuffered aqueous solution: Reassessing the roles of proton transfer and hydrogen bonding in the aqueous electrochemistry of quinones", *J. Am. Chem. Soc.* **129**, 12847 (2007). https://doi.org/10.1021/ja0743083
[10]S. Jin, M. Wu, R.G. Gordon, M.J. Aziz, and D.G. Kwabi, "pH swing cycle for CO_2 capture electrochemically driven through proton-coupled electron transfer", *Energy & Environmental Science* **13**, 3706 (2020). https://doi.org/10.1039/d0ee01834a
[11]H. Xie, W. Jiang, T. Liu, Y. Wu, Y. Wang, B. Chen, D. Niu, and B. Liang, "Low-energy electrochemical carbon dioxide capture based on a biological redox proton carrier", *Cell Reports Physical Science* **1**, (2020). https://doi.org/10.1016/j.xcrp.2020.100046
[12]B. Gurkan, F. Simeon, and T.A. Hatton, "Quinone reduction in ionic liquids for electrochemical CO_2 separation", *ACS Sustainable Chemistry & Engineering* **3**, 1394 (2015). https://doi.org/10.1021/acssuschemeng.5b00116
[13]D. Wielend, D.H. Apaydin, and N.S. Sariciftci, "Anthraquinone thin-film electrodes for reversible CO_2 capture and release", *Journal of Materials Chemistry A* **6**, 15095 (2018). https://doi.org/10.1039/c8ta04817g
[14]S. Voskian and T.A. Hatton, "Faradaic electro-swing reactive adsorption for CO_2 capture", *Energy & Environmental Science* **12**, 3530 (2019). https://doi.org/10.1039/c9ee02412c
[15]Y. Liu, H.Z. Ye, K.M. Diederichsen, T. Van Voorhis, and T.A. Hatton, "Electrochemically mediated carbon dioxide separation with quinone chemistry in salt-concentrated aqueous media", *Nat. Commun.* **11**, 2278 (2020). https://doi.org/10.1038/s41467-020-16150-7
[16]K.M. Diederichsen, Y. Liu, N. Ozbek, H. Seo, and T.A. Hatton, "Toward solvent-free continuous-flow electrochemically mediated carbon capture with high-concentration liquid quinone chemistry", *Joule* **6**, 221 (2022). https://doi.org/10.1016/j.joule.2021.12.001
[17]J.M. Barlow and J.Y. Yang, "Oxygen-stable electrochemical CO_2 capture and concentration with quinones using alcohol additives", *J. Am. Chem. Soc.* **144**, 14161 (2022). https://doi.org/10.1021/jacs.2c04044
[18]X. Li, X. Zhao, Y. Liu, T.A. Hatton, and Y. Liu, "Redox-tunable Lewis bases for electrochemical carbon dioxide capture", *Nature Energy* **7**, 1065 (2022). https://doi.org/10.1038/s41560-022-01137-z
[19]S. Jin, M. Wu, Y. Jing, R.G. Gordon, and M.J. Aziz, "Low energy carbon capture via electrochemically induced pH swing with electrochemical rebalancing", *Nat. Commun.* **13**, 2140 (2022). https://doi.org/10.1038/s41467-022-29791-7
[20]H. Seo and T.A. Hatton, "Electrochemical direct air capture of CO_2 using neutral red as reversible redox-active material", *Nat. Commun.* **14**, 313 (2023). https://doi.org/10.1038/s41467-023-35866-w
[21]S. Pang, S. Jin, F. Yang, M. Alberts, L. Li, D. Xi, R.G. Gordon, P. Wang, M.J. Aziz, and Y. Ji, "A phenazine-based high-capacity and high-stability electrochemical CO_2 capture cell with coupled electricity storage", *Nature Energy* (2023). https://doi.org/10.1038/s41560-023-01347-z
[22]C.L. Huang, C.J. Liu, K.J. Wu, H.R. Yue, S.Y. Tang, H.F. Lu, and B. Liang, "CO_2 capture from flue gas using an electrochemically reversible hydroquinone/quinone solution", *Energy & Fuels* **33**, 3380 (2019). https://doi.org/10.1021/acs.energyfuels.8b04419
[23]L. Luo, L. Hou, Y. Liu, K. Wu, Y. Zhu, H. Lu, and B. Liang, "Regeneration of Na_2Q in an electrochemical CO_2 capture system", *Energy & Fuels* **35**, 12260 (2021). https://doi.org/10.1021/acs.energyfuels.1c00960
[24]S. Jin, Y. Jing, D.G. Kwabi, Y. Ji, L. Tong, D. De Porcellinis, M.A. Goulet, D.A. Pollack, R.G. Gordon, and M.J. Aziz, "A water-miscible quinone flow battery with high volumetric capacity and energy density", *ACS Energy Letters* **4**, 1342 (2019). https://doi.org/10.1021/acsenergylett.9b00739

[25]Y. Ji, M.A. Goulet, D.A. Pollack, D.G. Kwabi, S. Jin, D. Porcellinis, E.F. Kerr, R.G. Gordon, and M.J. Aziz, "A phosphonate-functionalized quinone redox flow battery at near-neutral pH with record capacity retention rate", *Advanced Energy Materials* **9**, 1900039 (2019). https://doi.org/10.1002/aenm.201900039
[26]B.T. Huskinson, M.P. Marshak, C. Suh, S. Er, M.R. Gerhardt, C.J. Galvin, X. Chen, A. Aspuru-Guzik, R.G. Gordon, and M.J. Aziz, "A metal-free organic–inorganic aqueous flow battery", *Nature* **505**, 195 (2014). https://doi.org/10.1038/nature12909
[27]K. Lin, Q. Chen, M.R. Gerhardt, L. Tong, S.B. Kim, L. Eisenach, A.W. Valle, D. Hardee, R.G. Gordon, M.J. Aziz, and M.P. Marshak, "Alkaline quinone flow battery", *Science* **349**, 1529 (2015). https://doi.org/10.1126/science.aab3033
[28]D.G. Kwabi, K. Lin, Y. Ji, E.F. Kerr, M.-A. Goulet, D. De Porcellinis, D.P. Tabor, D.A. Pollack, A. Aspuru-Guzik, R.G. Gordon, and M.J. Aziz, "Alkaline quinone flow battery with long lifetime at pH 12", *Joule* **2**, 1907 (2018). https://doi.org/10.1016/j.joule.2018.08.013
[29]M. Wu, Y. Jing, A.A. Wong, E.M. Fell, S. Jin, Z. Tang, R.G. Gordon, and M.J. Aziz, "Extremely stable anthraquinone negolytes synthesized from common precursors", *Chem* **6**, 11 (2020). https://doi.org/10.1016/j.chempr.2020.03.021.
[30]Y. Jing, E.W. Zhao, M.A. Goulet, M. Bahari, E.M. Fell, S. Jin, A. Davoodi, E. Jonsson, M. Wu, C.P. Grey, R.G. Gordon, and M.J. Aziz, "In situ electrochemical recomposition of decomposed redox-active species in aqueous organic flow batteries", *Nat. Chem.* **14**, 1103 (2022). https://doi.org/10.1038/s41557-022-00967-4
[31]D.G. Kwabi, Y. Ji, and M.J. Aziz, "Electrolyte lifetime in aqueous organic redox flow batteries: A critical review", *Chem. Rev.* **120**, 6467 (2020). https://doi.org/10.1021/acs.chemrev.9b00599
[32]M. Wu, M. Bahari, E. Fell, R.G. Gordon, and M.J. Aziz, "High-performance anthraquinone with potentially low cost for aqueous redox flow batteries", *Journal of Materials Chemistry A* (2021). https://doi.org/10.1039/d1ta08900e
[33]E.F. Kerr, Z. Tang, T.Y. George, S. Jin, E.M. Fell, K. Amini, Y. Jing, M. Wu, R.G. Gordon, and M.J. Aziz, "High energy density aqueous flow battery utilizing extremely stable, branching-induced high-solubility anthraquinone near neutral pH", *ACS Energy Letters* **8**, 8 (2023). https://doi.org/https://doi.org/10.1021/acsenergylett.2c01691
[34]Y. Marcus, "Tetraalkylammonium ions in aqueous and non-aqueous solutions", *Journal of Solution Chemistry* **37**, 1071 (2008). https://doi.org/10.1007/s10953-008-9291-1
[35]Y. Zhu, Y. Li, Y. Qian, L. Zhang, J. Ye, X. Zhang, and Y. Zhao, "Anthraquinone-based anode material for aqueous redox flow batteries operating in nondemanding atmosphere", *Journal of Power Sources* **501**, (2021). https://doi.org/10.1016/j.jpowsour.2021.229984
[36]J. Seravalli and S.W. Ragsdale, "^{13}C NMR characterization of an exchange reaction between CO and CO_2 catalyzed by carbon monoxide dehydrogenase", *Biochemistry* **47**, 12 (2008). https://doi.org/https://doi.org/10.1021/bi8004522
[37]B. Hu, C. DeBruler, Z. Rhodes, and T.L. Liu, "Long-cycling aqueous organic redox flow battery (AORFB) toward sustainable and safe energy storage", *J. Am. Chem. Soc.* **139**, 1207 (2017). https://doi.org/10.1021/jacs.6b10984
[38]E.S. Beh, D. De Porcellinis, R.L. Gracia, K.T. Xia, R.G. Gordon, and M.J. Aziz, "A neutral pH aqueous organic–organometallic redox flow battery with extremely high capacity retention", *ACS Energy Letters* **2**, 639 (2017). https://doi.org/10.1021/acsenergylett.7b00019
[39]A.T. Bui, N.A. Hartley, A.J.W. Thom, and A.C. Forse, "Trade-off between redox potential and the strength of electrochemical CO_2 capture in quinones", *J. Phys. Chem. C Nanomater. Interfaces* **126**, 14163 (2022). https://doi.org/10.1021/acs.jpcc.2c03752
[40]A.M. Zito, D. Bím, S. Vargas, A.N. Alexandrova, and J.Y. Yang, "computational and experimental design of quinones for electrochemical CO_2 capture and concentration", *ACS Sustainable Chemistry & Engineering* **10**, 11387 (2022). https://doi.org/10.1021/acssuschemeng.2c03463